

Chemical and Crystallographic Characterization of the Tip Apex in Scanning Probe Microscopy

Thomas Hofmann, Florian Pielmeier, and Franz J. Giessibl*

Institute of Experimental and Applied Physics, University of Regensburg, D-93053 Regensburg, Germany

(Dated: December 3, 2024)

The apex atom of a W scanning probe tip reveals a non-spherical charge distribution as probed by a CO molecule bonded to a Cu(111) surface [Welker *et al.* Science, 336, 444 (2012)]. Three high-symmetry images were observed and related to three low-index crystallographic directions of the W bcc crystal. Open questions remained, such as the detectability of a contamination of W tips by sample material (here Cu), and the applicability of the method to distinguish other atomic species. In this work, we investigate bulk Cu and Fe tips. In both cases, we can associate our data with the fcc (Cu) and bcc (Fe) crystal structures using a simple electrostatic model that is based on the partial filling of d orbitals.

The front atom of the tip in a scanning probe microscope is important - it can be compared to the objective lens in an optical microscope. In scanning tunneling microscopy (STM), the tip can often be treated as spherically symmetric (Tersoff-Hamann s-wave model [1]). In atomic force microscopy, the front atom strongly affects both the appearance of imaged atoms [2] as well as force spectroscopy [3]. An indirect method to determine the tip cluster is the comparison of experimental results with *ab initio* calculations for different realistic tip models [4–6]. Another possibility is the combination of field ion microscopy (FIM), which can resolve the atomic structure of a sharp asperity [7], with an AFM [8, 9]. A common method is the functionalization of the tip apex with atoms or molecules picked up from the surface [10–15]. Carbon monoxide (CO) is commonly used, because its confined and closed-shell electronic structure makes it an inert probe for high-resolution atomic force imaging [11–13, 16]. Recently, a CO molecule, adsorbed on a Cu(111) surface, has been used to probe the apex atom of a W tip [2] - a technique introduced as **CO** Front atom Identification (COFI) [3].

In this Letter, we show that COFI images and force spectroscopy can be used to distinguish Cu front atoms from W and Fe front atoms and to determine their angular orientation. We further introduce an electrostatic model that relates the symmetries of experimental COFI images obtained with the Cu tips to the partial filling of d orbitals in the apex atom.

All measurements were performed in a low temperature STM/AFM operated at 4.4 K (LT STM/AFM, Omicron Nanotechnology, Taunusstein). The microscope is equipped with a qPlus sensor [17] and operated in the frequency modulation mode ($A = 50$ pm). We used qPlus sensors with tips etched from polycrystalline Cu (99.95 %), Fe (99.998 %) and W (99.95 %) wires. The measurements were conducted on a Cu(111) sample, which was covered by about 0.01 ML CO. Prior to the measurements on the CO/Cu(111) sample, all tips were cleaned *in situ* by field evaporation. The apex of the tip was altered by poking it into the Cu surface between im-

age acquisition. For modifying only the front-most part of the tip apex, the tip was approached by a few hundred picometers from the STM setpoint towards the clean Cu surface and then retracted while a bias between 0.5 and 5 V was applied [2, 18]. We call this procedure a gentle poke, in contrast to a strong poke where the tip is indented several nanometers into the surface. The latter is expected to result in a complete covering of the tip apex with sample material [19, 20].

During the measurements with the bulk Cu tips, the tip apex was modified repeatedly by strong and gentle pokes. After each poke, the tip atom was characterized by COFI [2, 3]. This involves the tip being scanned at close distance over the CO molecule, while the averaged force gradient $\langle k_{ts} \rangle$ is recorded. These close $\langle k_{ts} \rangle$ maps are referred to as ‘COFI images’ in the following. Among these COFI images [18] three high-symmetry images are identified (Fig. 1). Two are circular symmetric [Fig. 1(c) and 1(h)], the third one shows a twofold symmetry [Fig. 1(m)]. From the different contrast in the circular symmetric images, it is already apparent that they represent two different tip clusters. In addition, we obtained force versus distance curves at certain positions in the COFI images. Those recorded in the center of the circular symmetric images [Fig. 1(e) and 1(j)] exhibit a large difference in the magnitude of the force (150 vs. 30 pN) and in the z position of the attractive minimum and confirm that the COFI images represent two different tip clusters.

Calculations have shown that bulk tungsten displays a charge density that is significantly larger towards the neighboring atoms [21–23], while calculations for Cu predict a much more uniform electron distribution [24–27]. The strong angular force variations between a W tip and a CO molecule adsorbed on Cu(111) can be explained by the charge density of bulk W [2], while the experimental angular dependencies between Cu tips and CO molecules presented here cannot be explained by the bulk charge density of Cu. Therefore we develop a model for the Cu tip atom that relies on a partial depletion of the d-shell, leading to non-spherical electron distributions for

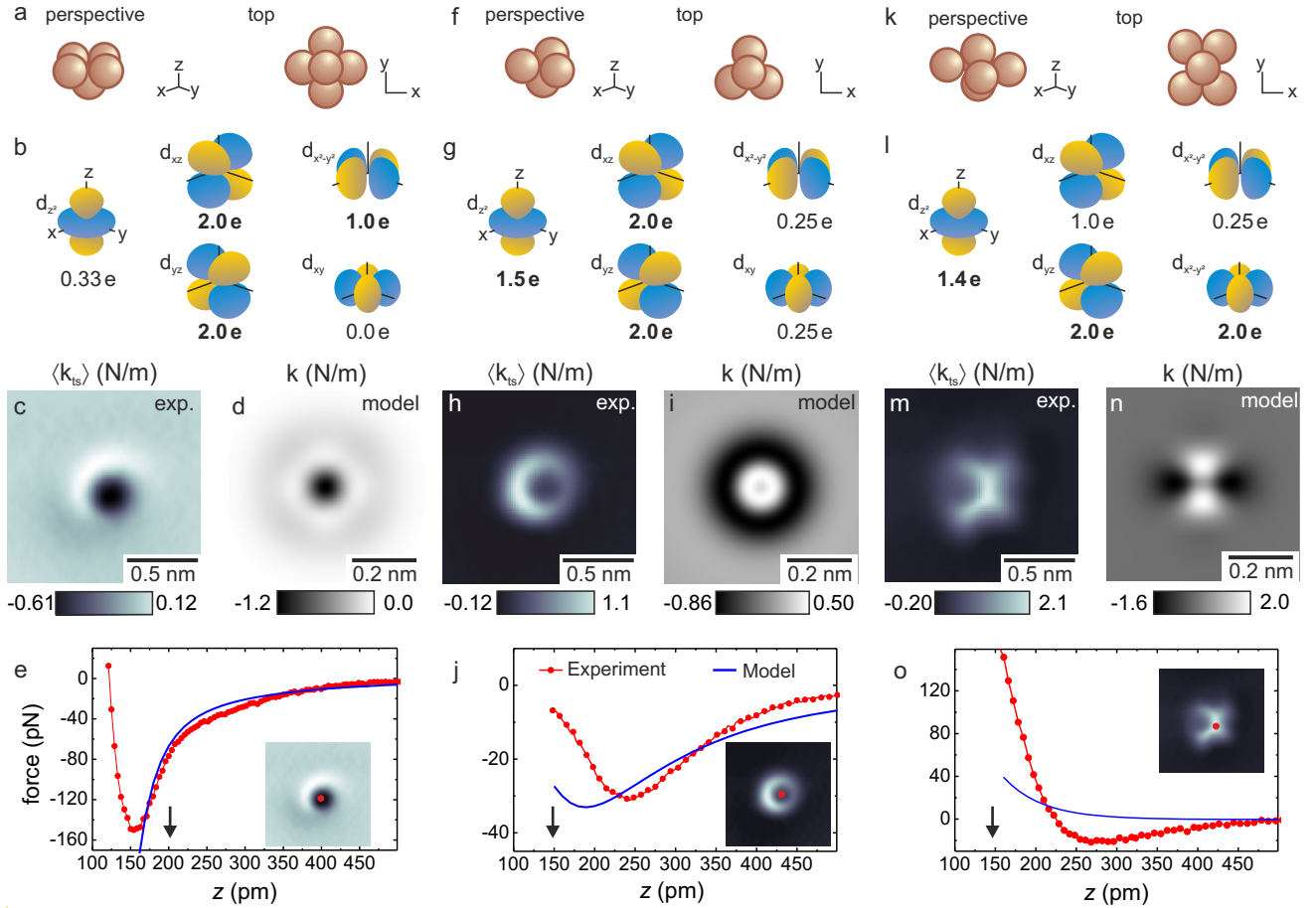


FIG. 1. (color online). Cu tips yield three high-symmetry COFI images (c, h and m), which can be assigned to Cu tip clusters pointing into the $\langle 100 \rangle$ (a), $\langle 111 \rangle$ (f) and $\langle 110 \rangle$ directions (k). To justify the assignment, we develop a model for the tip atom and calculate its electrostatic interaction with the dipole of the CO molecule. The model tip atom consists of a positive charge in the center, surrounded by unequally occupied 3d orbitals. Their occupation (b, g and l) is determined by their angular overlap with the nearest neighbors. The bold labels refer to the three orbitals with the highest occupation. The central charge is adjusted to optimize the fit between model and experimental results for the force versus distance behavior (e, j and o) and the contrast in the model images, which are calculated at a core-core distance of 200 (d), 145 (i) and 160 pm (n). The black arrows in the force versus distance graphs indicate the distances of the COFI images. The experimental distance is determined from the conductance of the tunneling gap [18]. In the model, the z -value reflects the core-core distance between the Cu tip atom and the oxygen [18].

tip clusters pointing into the high-symmetry orientations of a fcc crystal $\langle 100 \rangle$, $\langle 111 \rangle$ and $\langle 110 \rangle$ (Fig. 1). The model explains the experimental observations of toroidal COFI images [Fig. 1(c) and 1(h)] for Cu $\langle 100 \rangle$ and Cu $\langle 111 \rangle$ tips and ‘rooftop’-type COFI images for Cu $\langle 110 \rangle$ tips [Fig. 1(m)].

Density functional calculations of metal tips confirm that the Smoluchowski effect [28] leads to a surface dipole at the tip atom [5]. For a Cu adatom on a Cu(111) surface the same effect has been reported [20] and calculations show that the occupation of the 4s and 3d orbitals is reduced compared to an isolated Cu atom [29]. In a homogeneous electric field, the 3d orbitals are degenerate and the field would deplete (or fill) the orbitals equally. However, the field around a Cu tip atom is expected to be strongly inhomogeneous due to the partially unscreened

nuclei of the nearest neighbors [30, 31] and the energy levels of the 3d orbitals split up according to crystal field theory [32]. This leads to an unequal depletion of the 3d orbitals and correspondingly, a non-spherical charge density around the Cu tip atom.

Following these arguments, we model the electron distribution at the Cu tip atom by 3d orbitals. Contributions of s or p states are not included. The occupation of the 3d orbitals is estimated by the angular overlap of each orbital with all nearest neighbors [33], assuming that orbitals with a large overlap are lower in energy and, hence, carry a higher occupation (for more details and a discussion of the occupation numbers see [18]). The occupation of the orbitals determines the basic features found in the COFI images: In the case of the Cu $\langle 100 \rangle$ tips [Fig. 1(b)] the electron distribution has the shape of a torus be-

cause the d_{xz} and d_{yz} orbitals are fully occupied. The same holds true for the Cu $\langle 111 \rangle$ tips [Fig. 1(g)] but the torus shows a shallower minimum in the center than the Cu $\langle 100 \rangle$ tips because the d_{z^2} orbital is also highly populated. The asymmetry in the occupation of the d_{xz} and d_{yz} orbitals found for the Cu $\langle 110 \rangle$ tips [Fig. 1(l)] results in a twofold symmetry which is reflected in the COFI image in Fig. 1(m).

For a quantitative comparison of the experiment and the tip model, the interaction of the electron distribution and the CO molecule is estimated by electrostatics, as discussed in Ref. [2]. The CO molecule is considered as a dipole with a negative charge on the oxygen atom and a realistic dipole moment of about $0.1 \text{ e} \cdot 100 \text{ pm}$ [34, 35]. The negative charge of the electron distribution at the tip atom is compensated by a positive charge Q_{core} in the center. In order to approximately match the contrast in the COFI images and the characteristics of the force versus distance curves, the magnitude of the positive charge is adjusted. As a result, the net charge of the tip atoms $\Delta = Q_{\text{core}} - Q_{3d \text{ elec.}}$ is positive for all tip orientations, with $\Delta_{100} = +0.25 \text{ e}$, $\Delta_{111} = +0.52 \text{ e}$ and $\Delta_{110} = +0.04 \text{ e}$. Calculations of the dipole moment of a metal tip atom yield a value of approximately $0.4 \text{ e} \cdot 100 \text{ pm}$ [5]. This corresponds to a charge of $+0.2 \text{ e}$ at the tip atom assuming a distance of 200 pm between the charges, indicating that our estimative model returns a realistic net charge at the tip atom.

The calculated image of the Cu $\langle 100 \rangle$ tip shows a toroidal symmetry with a strong attraction in the center [Fig. 1(d)], whereas the image of the Cu $\langle 111 \rangle$ tip only reveals a small attractive dip [Fig. 1(i)]. As the experimental toroidal COFI images fall into two categories (large dip in Fig. 1(c) and small dip in Fig. 1(h)), they can be unambiguously identified as Cu $\langle 100 \rangle$ and Cu $\langle 111 \rangle$ tips with the help of the model. The calculation for the Cu $\langle 110 \rangle$ tip [Fig. 1(n)] yields a twofold symmetric image similar to the COFI image in Fig. 1(m). This result supports the assignment based on the symmetry. Notably, the experimental tip images are more than 2.5 times the size of the calculated images. This is explained by the bending of the CO molecule that is known to magnify the image of the tip atom [3] or the length of intermolecular bonds [36] and which is not considered in the calculations.

The measurements with Fe tips again reveal three high-symmetry COFI images [Figs. 2(b), 3(c) and 3(d)]. These exhibit the same symmetries as the W tips [Figs. 2(a), 3(a) and 3(b)] and are therefore assigned to tips oriented in $\langle 100 \rangle$, $\langle 110 \rangle$ and $\langle 111 \rangle$ direction. Similar to W, Fe has a partially filled d shell and a bcc bulk crystal structure, suggesting a higher electron density in the $\langle 111 \rangle$ directions, where the nearest neighbors are located. However, calculations of the total charge density in Fe are not conclusive. In Refs. [37, 38] a spherical charge density around the Fe atoms is revealed and no increase in direction of

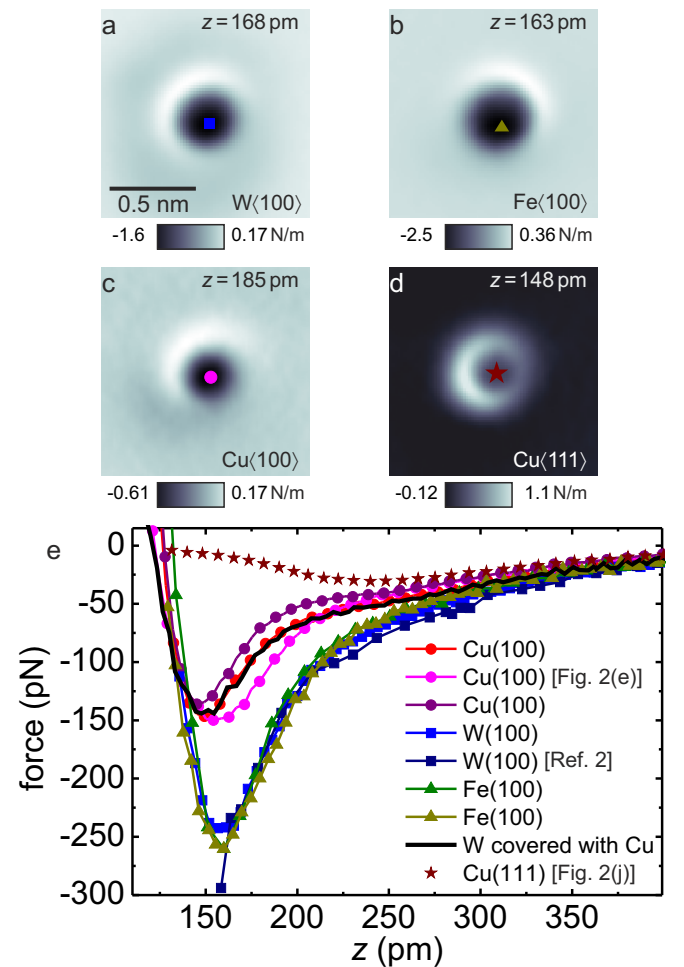


FIG. 2. (color online). Comparison of W (a), Fe (b) and Cu tips (c and d), which show a circular symmetry in the COFI image (c and d are the same as in Fig. 1). e) Force versus distance curves of W $\langle 100 \rangle$ (squares), Fe $\langle 100 \rangle$ tips (triangles), Cu $\langle 100 \rangle$ (circle) and Cu $\langle 111 \rangle$ tips (stars). The solid (black) line represents a W tip, which is contaminated with Cu.

the nearest neighbors is resolved, while a more recent calculation reports a non-spherical electron density [39].

In order to evaluate the potential of the COFI method to distinguish between different chemical species at the tip apex, we compare COFI images and force versus distance curves of Cu, Fe and W tips. The comparison is divided into tips which reveal circular symmetric COFI images (Fig. 2), and tips that exhibit a two- or threefold symmetry (Fig. 3).

Toroidal symmetric COFI images are observed for W, Fe and Cu tips oriented in $\langle 100 \rangle$ direction, and a Cu $\langle 111 \rangle$ tip [Fig. 2(a)-(d)]. The Cu $\langle 111 \rangle$ tip can easily be distinguished from all other tips by the contrast in the COFI images and its force versus distance curve [Fig. 2(e)]. The COFI images of the $\langle 100 \rangle$ tips do not allow a discrimination. The force versus distance curves obtained with three different Cu $\langle 100 \rangle$ tips, however, show a significantly

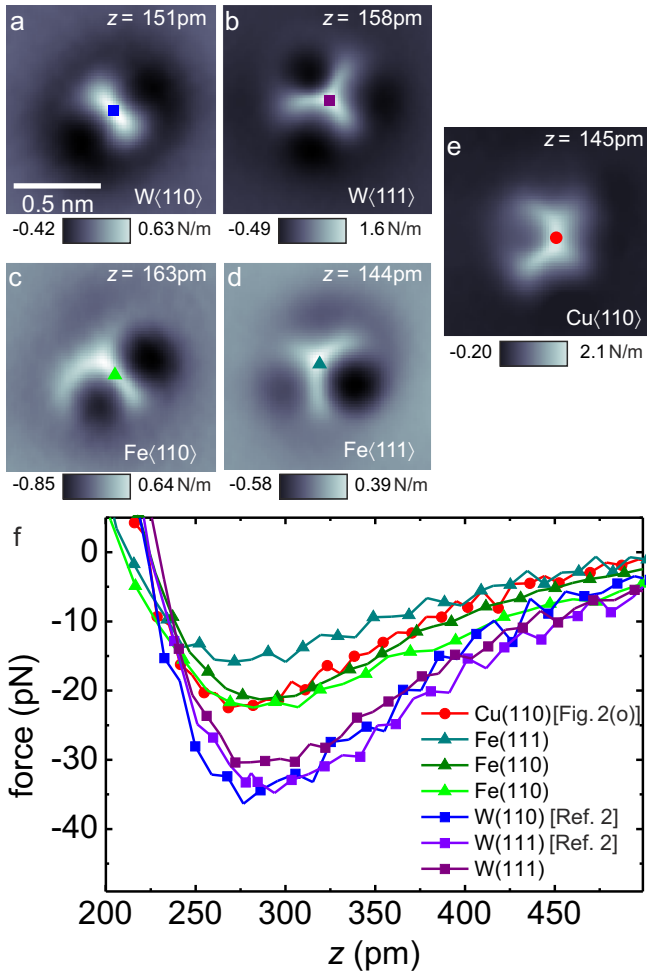


FIG. 3. (color online). Comparison of W, Fe and Cu tips revealing two- or threefold symmetry. a-e) COFI images of the corresponding W (a, b), Fe (c, d) and Cu tips (e) (a is reproduced from [2], e is the same as in Fig. 1(i)). f) Force versus distance curves of several W, Fe and Cu tips.

smaller maximal attractive force (130 – 150 pN, variation explained in [18]) than those obtained with Fe(100) and W(100) tips (≈ 250 pN). It is therefore possible to distinguish Cu from Fe and W tips for the $\langle 100 \rangle$ orientations. To support this finding, we modified a W tip apex by several hard pokes into the Cu surface. The COFI image after the modification revealed the image of a tip oriented in $\langle 100 \rangle$ direction. The comparison of its force versus distance curve [black line in Fig. 2(e)] with curves of Cu(100) and W(100) tips clearly reveals a decoration of the W tip apex with Cu. This is expected for such tip treatment [19, 20] and proves the capability of COFI to identify a covering of the tip apex with Cu.

In Fig. 3, examples of COFI images of W, Fe and Cu tips with two- and threefold symmetry are presented. COFI images of W, Fe and Cu tips, oriented in $\langle 110 \rangle$ -direction are all twofold symmetric, but the image of the Cu tip [Fig. 3(e)] is significantly different from those of W

[Fig. 3(a)] and Fe [Fig. 3(c)]. The Cu tip image features a repulsive part with the shape of a ‘rooftop’ with four shallow minima, whereas the W/Fe tip images exhibit a repulsive bar with two highly attractive minima. Therefore a Cu(110) tip can be unambiguously identified by the COFI image. As expected, W and Fe tips cannot be distinguished from the qualitative COFI image, as both are bcc crystals.

However, the force versus distance curves of the two- and threefold symmetric tips [Fig. 3(f)] recorded at the repulsive maximum in the COFI images do allow to distinguish W and Fe tips. We find that curves recorded with W(110) and W(111) tips are almost identical, exhibiting a force minimum between 30 and 35 pN. The curves of the Fe(110) and Fe(111) tips, on the other hand, show a smaller attractive minimum of 15 to 22 pN. Therefore Fe and W can be distinguished with the help of the force versus distance curves. The greater deviation between the force minimum of the Fe(110) and Fe(111) tips is probably due to a greater misalignment to the precise $\langle 110 \rangle$ and $\langle 111 \rangle$ orientations. The angular deviations are smaller for the W tips shown in Fig. 3(a) and 3(b). For details on the effect of angular alignments, see Fig. S 9 in Ref. [2].

In conclusion, we report three high-symmetry COFI images for Cu and Fe, which can be related to the high-symmetry directions of the fcc and bcc crystals. We therefore suggest that in almost all cases the tip clusters exhibit a bulk-like crystal structure. A tip model based on the partial depletion of selected d orbitals can qualitatively explain the observed COFI images. However, for a quantitative description *ab initio* calculations may be helpful, similar to those calculated for W tips [40]. The comparison of the results for W, Fe and Cu tips reveals that COFI is a powerful method to distinguish between the orientation as well as the chemical species of the tip atom. The method has been proven to be useful for measurements on various samples like Si [3], NiO [41] and graphene [42].

The authors thank A. J. Weymouth, L. Gross and J. Repp for discussions and kindly acknowledge financial support from the Deutsche Forschungsgemeinschaft (Grant No. GRK 1570).

* franz.giessibl@ur.de

- [1] J. Tersoff, D. R. Hamann, *Phys. Rev. Lett.* **50**, 1998 (1983).
- [2] J. Welker, F. J. Giessibl, *Science* **336**, 444 (2012).
- [3] J. Welker, A. J. Weymouth, F. J. Giessibl, *ACS Nano* **7**, 7377 (2013).
- [4] Y. Sugimoto, P. Pou, M. Abe, P. Jelinek, R. Pérez, S. Morita, O. Custance, *Nature*, **446**, 64 (2007).
- [5] G. Teobaldi, K. Lämmle, T. Trevethan, M. Watkins, A. Schwarz, R. Wiesendanger, A. L. Shluger, *Phys. Rev.*

Lett. **106**, 216102 (2011).

[6] M. Ternes, C. González, C. P. Lutz, P. Hapala, F. J. Giessibl, P. Jelínek, A. J. Heinrich, *Phys. Rev. Lett.* **106**, 016802 (2011).

[7] E. W. Müller, *Zeitschrift für Physik* **131**, 136 (1951).

[8] J. Falter, G. Langewisch, H. Hölscher, H. Fuchs, A. Schirmeisen, *Phys. Rev. B* **87**, 115412 (2013).

[9] W. Paul, D. Oliver, Y. Miyahara, P. H. Grütter, *Phys. Rev. Lett.* **110**, 135506 (2013).

[10] L. Bartels, G. Meyer, K.-H. Rieder, D. Velic, E. Knoesel, A. Hotzel, M. Wolf, G. Ertl *Phys. Rev. Lett.* **80**, 2004 (1998).

[11] L. Gross, F. Mohn, N. Moll, P. Liljeroth, G. Meyer, *Science* **325**, 1110 (2009).

[12] N. Pavliček, B. Fleury, M. Neu, J. Niedenführ, C. Herranz-Lancho, M. Ruben, J. Repp, *Phys. Rev. Lett.* **108**, 086101 (2012).

[13] M. P. Boneschanscher, J. van der Lit, Z. Sun, I. Swart, P. Liljeroth, D. Vanmaekelbergh, *ACS Nano* **6**, 10216 (2012).

[14] G. Kichin, C. Wagner, F. S. Tautz, R. Temirov, *Phys. Rev. B* **87**, 081408 (2013).

[15] F. Mohn, B. Schuler, L. Gross, G. Meyer, *Appl. Phys. Lett.* **102**, 073109 (2013).

[16] Z. Sun, M. P. Boneschanscher, I. Swart, D. Vanmaekelbergh, P. Liljeroth, *Phys. Rev. Lett.* **106**, 046104 (2011).

[17] F. J. Giessibl, *Appl. Phys. Lett.* **73**, 3956 (1998).

[18] See Supplemental Materials for details about the tip manipulation, data acquisition and analysis, Cu tip model, effect of COFI on the current and more COFI images of Cu tips.

[19] S.-W. Hla, K.-F. Braun, V. Iancu, A. Deshpande, *Nano Lett.* **4**, 1997 (2004).

[20] L. Limot, J. Kröger, R. Berndt, A. Garcia-Lekue, W. A. Hofer, *Phys. Rev. Lett.* **94**, 126102 (2005).

[21] M. Posternak, H. Krakauer, A. J. Freeman, D. D. Koelling, *Phys. Rev. B* **21**, 5601 (1980).

[22] L. F. Mattheiss, D. R. Hamann, *Phys. Rev. B* **29**, 5372 (1984).

[23] C. A. Wright, S. D. Solares, *Nano letters* **11**, 5026 (2011).

[24] C. Fong, J. Walter, M. Cohen, *Physical Review B* **11**, 2759 (1975).

[25] J. Gay, J. Smith, F. Arlinghaus, *Phys. Rev. Lett.* **38**, 561 (1977).

[26] A. Euceda, D. M. Bylander, L. Kleinman, K. Mednick, *Physical Review B* **27**, 659 (1983).

[27] A. Euceda, D. M. Bylander, L. Kleinman, *Physical Review B* **28**, 528 (1983).

[28] R. Smoluchowski, *Phys. Rev.* **60**, 661 (1941).

[29] J. A. Rodriguez, M. Kuhn, *The Journal of Physical Chemistry* **98**, 11251 (1994).

[30] P. Rao, J. Waber, *Surface Science* **28**, 299 (1971).

[31] J. Herbst, *Phys. Rev. B* **15**, 3720 (1977).

[32] J. Van Vleck, *Phys. Rev.* **41**, 208 (1932).

[33] C. E. Schäffer, C. K. Jørgensen, *Molecular Physics* **9**, 401 (1965).

[34] Z. Zuo, W. Huang, P. Han, Z. Li, *Journal of molecular modeling* **15**, 1079 (2009).

[35] M. Feng, P. Cabrera-Sanfelix, C. Lin, A. Arnau, D. Sánchez-Portal, J. Zhao, P. M. Echenique, H. Petek, *ACS nano* **5**, 8877 (2011).

[36] L. Gross, F. Mohn, N. Moll, B. Schuler, A. Criado, E. Gutián, D. Peña, A. Gourdon, G. Meyer, *Science* **337**, 1326 (2012).

[37] C. S. Wang, A. J. Freeman, *Phys. Rev. B* **24**, 4364 (1981).

[38] R. Wu, A. J. Freeman, *Phys. Rev. B* **47**, 3904 (1993).

[39] T. Jones, M. Eberhart, D. Clougherty, *Phys. Rev. Lett.* **100**, 017208 (2008).

[40] C. A. Wright, S. D. Solares, *Journal of Physics D: Applied Physics* **46**, 155307 (2013).

[41] F. Pielmeier, F. J. Giessibl *Phys. Rev. Lett.* **110**, 266101 (2013).

[42] T. Hofmann, A. J. Weymouth, A. Donarini, F. J. Giessibl, in preparation.

Supplemental Information

Chemical and Crystallographic Characterization of the Tip Apex in Scanning Probe Microscopy

Thomas Hofmann, Florian Pielmeier, and Franz J. Giessibl

Institute of Experimental and Applied Physics, University of Regensburg, D-93053 Regensburg, Germany

S 1 Modification and characterization of the tip apex

Prior to the measurements on the CO/Cu(111) sample, the tips of the force sensors were inserted in the field ion microscope that is part of the ultrahigh vacuum system which also contains the low temperature scanning tunneling/atomic force microscope (LT STM/AFM). Tips were cleaned by field evaporation with a voltage of up to 15 kV and transferred *in situ* to the LT STM/AFM. This is a standard procedure for cleaning tips in a field ion microscope [1] and allows for complete removal of the native oxide layer. Stable tunneling was observed with all tips directly after the approach to the Cu(111) surface.

During the characterization measurements the tip apex was modified by poking it into the Cu surface. We distinguish two kinds of pokes. Indenting the tip several nanometers into the metallic sample surface is defined as a strong poke. This is a standard procedure within the low temperature scanning tunneling microscopy community to prepare stable and reliable tips [2–4]. Strong pokes lead to craters in the sample surface with a depth of several nanometers. The result of a strong poke on the Cu surface is shown in Fig. S 1. In this example, the tip was approached 20 nm towards the surface. It has been assumed within the low temperature STM community that strong pokes in soft

metals such as Cu lead to a wetting of the tip by sample material [5]. Indeed, we could confirm that W tips are usually covered by Cu after performing strong pokes on a Cu sample by the tip identification methods outlined in this manuscript.

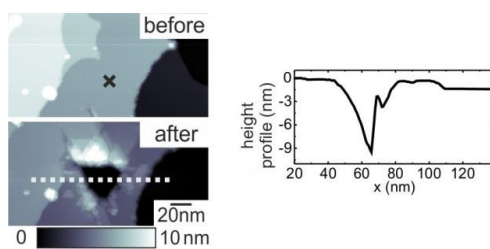


Fig. S 1 STM overview images before and after a strong poke. The poke involved a 20 nm advance of the tip towards the sample at the position marked by an 'x'. The height profile through the minimum of the poke site on the right (its trace is shown as a dotted line in the left bottom image) reveals that the strong poke resulted in a crater with a depth of almost 10 nm.

In contrast to strong pokes, gentle pokes can merely lead to recrystallizations of the front-most part of the tip apex without a material transfer from sample to tip or vice versa [6]. For a gentle poke, the tip is positioned above the clean Cu surface in STM feedback (current setpoint: 100 pA, bias: -10 mV). The corresponding tunneling resistance of 100 M Ω (a conductance of 10 nS) corresponds to a distance of about 420 pm from point contact over the Cu

surface (see section S 2), where the quantum point contact resistance of $12.9\text{ k}\Omega$ holds. The tip is approached between 400 to 900 pm and then retracted while a bias voltage between 0.5 and 5 V is applied. Before and after each gentle poke, a STM overview image is recorded. Additionally, the tip apex is characterized by COFI before and after each poke. Fig. S 2 a illustrates the sequence of characterizing and manipulating the tip apex. The details of COFI images are given in section S 2.

Fig. S 2 b-d schematically illustrates the three possible effects of gentle pokes on the sample surface and on the tip apices. The STM overview images before and after reveal the effects of the pokes on the sample surface. The poke sites are indicated by an 'x'. It is important to note that usually the STM images do not change significantly after pokes; however, the COFI images that show the force channel clearly reflect how the poke changed the tip apex.

The example in Fig. S 2 b represents the most common result of a gentle poke, i.e. one or several small bumps on the surface. These consist of single or multiple atoms which have been deposited from the tip. In Fig. S 2 b, the COFI image of the tip apex has changed from a twofold to a toroidal symmetry, indicating that the orientation of the tip cluster has changed. Generally, it is assumed that atoms released from the tip are surface atoms which were picked up beforehand during tip

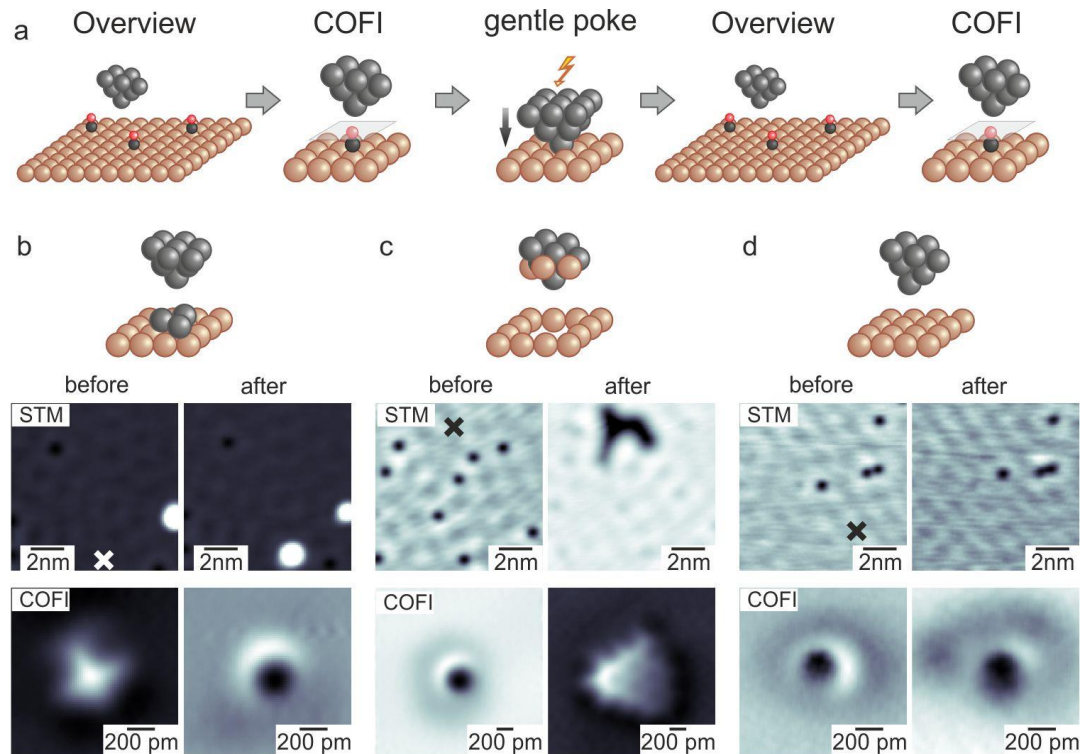


Fig. S 2 a) Sequence of a typical measurement: Before and after each poke, a STM overview image ($10\times10\text{ nm}^2$) and a COFI image are recorded. The overview image reveals the effect of the poke on the sample surface. A change of the tip cluster is identified by the COFI images. The pokes can result in a bump (b) or a void (c) on the surface. In rare cases, the surface is not affected by the poke (d), although the tip cluster has changed. The bump in the before image in (b) originates from a previous poke. The COFI image after the poke in (c) shows a tip cluster that is terminated by a small, triangular terrace (see description in the text). Note that the area of the COFI images is $2\times2\text{ nm}^2$ in (c), in contrast to $1.5\times1.5\text{ nm}^2$ in (b) and (d).

preparation by indentation [2,3,5]. But it is also possible that the bumps consist of atoms from the tip material.

Fig. S 2 c shows that a poke can also lead to a void in the surface. In this case Cu atoms are transferred from the sample to the tip. Before poking, the COFI image showed a toroidal tip image. Afterwards the COFI image revealed a triangle whose size is larger than the tip image of a single atom tip. A hexagonal lattice with six minima is visible within the triangle indicating that the tip is terminated by a triangular terrace of about six atoms. The atomic spacing is close to the nearest neighbor distance in Cu ($d_{NN} = 255$ pm), and the void created by the poke suggests that the tip-terminating triangular terrace consists of Cu. As the bulk tip material was W in this example, the Cu atoms at the tip apex were picked up from the surface. However, in general the adsorbed atoms must not necessarily end up at the tip apex but might also diffuse to the side of the tip.

In rare cases, gentle pokes alter the tip cluster without affecting the sample surface, i.e. neither is sample material picked up from the tip, nor are atoms originating from the tip dropped to the surface (see Fig. S 2 d or the tips 1, 2 and 3 presented in Ref. [6]). The STM overview image before and after the poke shows neither a protrusion nor a depression. However, the apparent depth of the CO molecules is different in the two images and the two neighboring CO molecules are resolved more clearly in the image recorded before the poke. These observations already suggest that the tip cluster has changed. The COFI images support this claim, as they show two different circular symmetric tips.

S 2 Acquisition and analysis of the COFI images and force versus distance curves

In FM-AFM, the key observable is the frequency shift Δf which directly corresponds to an averaged force gradient $\langle k_{ts} \rangle = \Delta f/f_0 \times 2k$. This allows to compare the physics of measurements (average force gradients) obtained with sensors that have alternate resonance frequencies f_0 and stiffnesses k . In the following table, the parameters of all sensors (f_0 , k and the quality factor Q) are shown:

Measurement type	k (N/m)	f_0 (Hz)	Q
All Cu tips	1800	26968.8	134705
Fe<100>-1	1800	59368.9	355500
Fe<100>-2	1800	23899.7	27280
Fe<110>-1	1800	28030.8	22025
Fe<110>-2	1800	59369.4	1120100
Fe<111>-1	1800	28030.9	20500
W<100>-1	1800	27845.7	28305
W<111>-1	1800	27846.6	28305

In addition to the force gradient $\langle k_{ts} \rangle$, the tunneling current is collected simultaneously. As the tip oscillates the tunneling current is averaged over several oscillation cycles. The sample voltage was set to -10 mV in all measurements.

The COFI image is the $\langle k_{ts} \rangle$ map that is recorded in constant height (CH) mode at a tip-sample distance close to the manipulation distance. This distance is determined experimentally by reducing the tip-sample distance in 10 pm steps until the CO is manipulated during imaging. At the distance of the COFI image the averaged tunneling current above the bare Cu surface is between 15 to 25 nA,

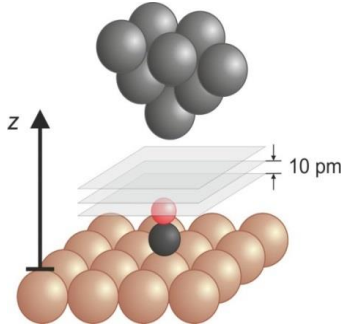


Fig. S 3 Acquisition of the constant height maps for the 3D force spectroscopy

corresponding to an average gap resistance of 333 to 400 k Ω . The COFI images only display the short range force components. The long range forces are subtracted. For this purpose, an averaged $\langle k_{ts} \rangle$ value is determined over the Cu surface. As we do not observe atomic resolution on the Cu surface, this value is attributed to long-range forces and therefore subtracted as a long range background from all image data, as proposed in Ref. [7].

The force distance curves are obtained either from a three-dimensional $\langle k_{ts} \rangle$ dataset or from point spectroscopy. For the 3D $\langle k_{ts} \rangle$ dataset, multiple CH maps are recorded by subsequently increasing the tip-sample distance in increments of 10 pm, starting with the closest distance where the COFI image was

taken. The distance is increased until the contrast difference between Cu and CO vanishes completely, typically at a height increase of about 0.5 nm. Hence, we usually record 50 maps and each map takes about 8 min. This sums up to a total of about 6.5 h acquisition time for a three dimensional data set. During this time, the feedback is switched off and the system is subject to thermal drift and piezo creep. The drift in the x- and y-directions is corrected by cross-correlating the current images over the whole distance range. The drift in z-direction is corrected with the help of fast current versus distance curves. These curves are acquired by point spectroscopy before or after the maps over the clean Cu surface at a fast speed where creep and drift are negligible. The curves are fitted by an exponential function with a decay constant κ , yielding a precise current versus height reference. The decay constant is used to determine the tip-sample distance from the tunneling current for each map, as explained in detail in section S 3. As in the case of the COFI image, the contribution of long range forces is subtracted in each $\langle k_{ts} \rangle$ map. Afterwards the 3D $\langle k_{ts} \rangle$ data set is deconvolved with the help of the Sader-Jarvis method [8] to obtain the 3D data set of the short range forces.

The point spectroscopy is acquired by retracting the tip by a distance of 800 pm with a velocity of 25 pm/s while $\langle k_{ts} \rangle(z)$ is recorded. For $\langle 100 \rangle$ tips, the minima in the $\langle k_{ts} \rangle(z)$ curves can only be observed by point spectroscopy. The reason is that the lateral forces exceed the manipulation threshold when moving the tip over the CO molecule at the distance where the vertical force minimum occurs. In addition to each point spectrum recorded over CO, a complementary one is recorded over the Cu surface. The $\langle k_{ts} \rangle(z)$ curve over Cu is subtracted from the one recorded over the CO molecule to remove the contribution of the long range forces. The resulting $\langle k_{ts} \rangle(z)$ curve is deconvolved by the method of Sader and Jarvis [8] to determine the force distance curve.

S 3 Determination of the tip-sample distance

If we assume that the tunneling current is dominated by a single apex atom, we can reference the tip-sample distance z at the lower turnaround point of the oscillation to quantum point contact with the conductivity $G_0 = 2e^2/h$ with the help of the following equation [6]:

$$z = \frac{1}{2\kappa} \ln \left(\frac{\langle I(z) \rangle}{I_0^{\text{Bessel}}(2\kappa A) \cdot G_0 \cdot V_{\text{sample}}} \right) - A, \quad (1)$$

with the Bessel function of order zero $I_0^{\text{Bessel}}(2\kappa A)$ and the current decay constant κ . The Bessel function is used to calculate the maximum tunneling current at the lower turnaround point from $\langle I(z) \rangle$, which is averaged over the oscillation cycle. The decay constant κ is determined from current point spectra by fitting an exponential decay to the current versus distance curve. We obtain values between 9.6 nm^{-1} and 10 nm^{-1} , which are typical for metal-metal tunneling gaps.

However, we found that $\langle k_{\text{ts}} \rangle(z)$ curves of tips with the same orientation can be offset by values as great as 50 pm. The reason is that the tunneling current does not only originate from the front atom but also contributions from atoms of the second tip layer are measured. As an effect, blunt tips yield a larger current compared to sharp tips if both are held at the same front-atom to sample distance. The sharpness of the tip can be estimated by the apparent depth of the CO molecule (Fig. S 4 a), measured at a moderate tip-sample distance – e.g. $I_{\text{set}} = 100 \text{ pA}$, $V_{\text{sample}} = -10 \text{ mV}$ – to avoid an influence of the forces between the tip atom and the CO molecule. Evaluating all measurements, we found a maximum depth $C_{\text{sharp}} = 43 \text{ pm}$. This value is taken as a reference for correcting the tip-sample distance in the force versus distance curves, which were obtained with tips which show a smaller apparent depth C_{blunt} . Assuming that the decay constant has the same value over CO and over the Cu(111) surface, we can renormalize the current measured with a blunt tip I_{blunt} with the help of the difference in the observed apparent depth $\Delta C = C_{\text{blunt}} - C_{\text{sharp}}$:

$$I_{\text{blunt}} = I_{\text{sharp}} \times \exp(-2\kappa\Delta C) \quad (2)$$

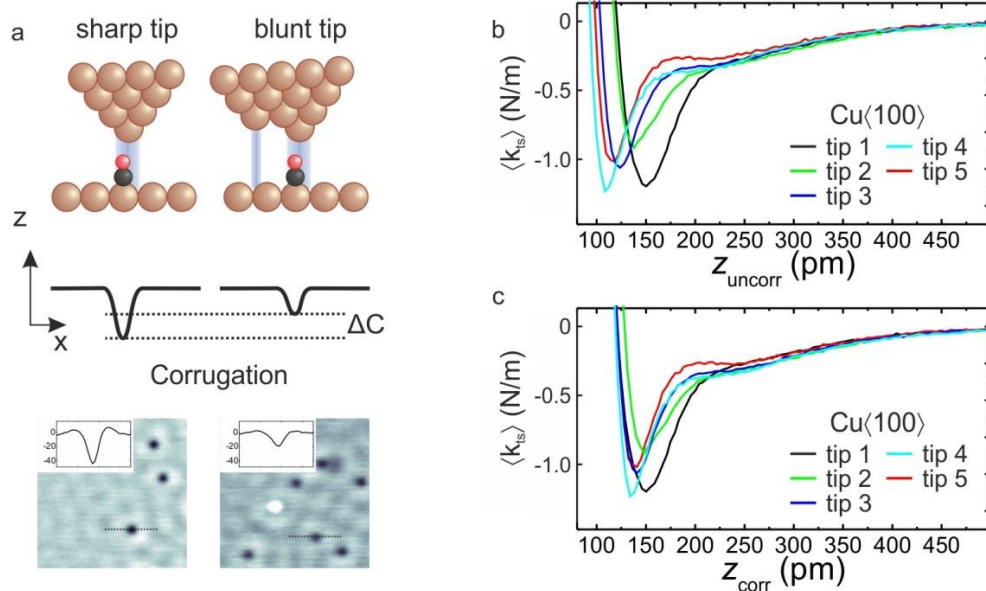


Fig. S 4 a) Illustration of the influence of a sharp compared to a blunt tip on the corrugation of the CO molecules. Parameters in the topography images: $I_{\text{set}} = 100 \text{ pA}$, $V_{\text{sample}} = -10 \text{ mV}$. Blunt tips (i.e. tip 3 - 5) yield negative z-offsets in the uncorrected frequency shift-distance curves (b), while a sharp tip (tip 1) does not show a z-offset. This can be corrected by subtraction of ΔC .

By combining equation (1) and (2), we find that the correct z -values can be calculated by the difference in the corrugations ΔC :

$$z_{\text{corr}} = z_{\text{uncorr}} + \Delta C \quad (3)$$

Fig. S 4 displays a set of curves obtained with different Cu<100> tips before (b) and after the correction of the z -values (c), showing that the correction algorithm leads to less scattering in $\langle k_{ts} \rangle(z)$ curves. The same correction algorithm is also used for all other tips, assuming that the topography image at large tip-sample distance is not influenced by the orientation and chemical nature of the tip.

S 4 Variations in the force versus distance curves of Cu <100> tips due to various tip tilt angles

Fig. S 5 c shows the force versus distance curves of the three Cu <100> tips from Fig. 2 in the main text again. The position and the value of the force minimum as well as the shape of the force versus distance curves vary, although all curves are recorded with Cu tips oriented in the <100> direction. We conjecture that this variation is caused by slight variations of the tilt of the tip from a perfect <100> alignment. Fig. S 5 b displays profile curves through the COFI images (Fig. S 5 a) of the three tips. An asymmetry in the profiles is a measure for the tilt out of the <100> direction. We find that tip 1 shows the smallest tilt, while tip 2 is strongly tilted. Apparently, the tilt leads to a shift of the force minimum towards smaller z values. In addition, the valley around the force minimum becomes narrower and a shoulder develops at a z value of approximately 200 pm.

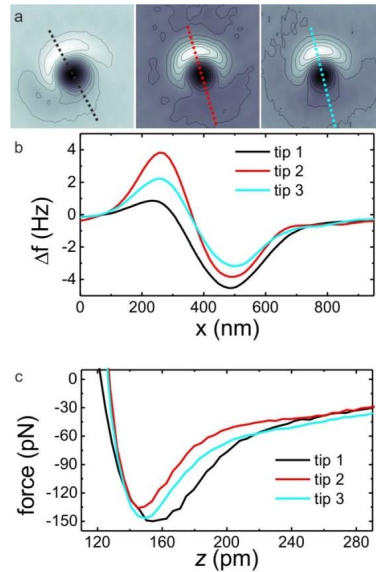


Fig. S 5 Influence of the tilt of Cu <100> tips on the shape of force versus distance curves: a) constant height frequency shift maps of tip 1, 2 and 3 with contour lines. b) Profile lines extracted from the COFI image at the position of the dotted lines (a). c) Force versus distance curves.

S 5 Development of an electrostatic model that describes the orientation-dependent interaction of the Cu tip with the CO molecule

A simple electrostatic model was developed to explain the COFI images obtained with the Cu tips. With the help of the model the COFI images can be assigned to the three low-index high-symmetry directions of the Cu fcc crystal. In the following, the model is explained in detail.

First, we determine an electron distribution at the tip atom for the three highly symmetric tip clusters in Fig. S 6 b, namely the $\langle 100 \rangle$, $\langle 111 \rangle$ and $\langle 110 \rangle$ orientations. We then calculate the electrostatic interaction force with the CO molecule, assuming a dipole moment of the CO molecule as proposed in Ref. [6].

The electronic states of the tip atom are approximated by atomic orbitals. We only consider the 3d orbitals because these show the directionality needed to explain the COFI images. All other orbitals are neglected. The 3d orbitals are described by Slater-type orbitals (STO) which have the following form (after [9], in SI units):

$$\Psi_{\text{STO}}^{d_i} = \sqrt{\frac{8}{45}} \chi^3 \frac{5}{a_B^{1.5}} \frac{r^2}{a_B^2} \exp\left(-\frac{\chi r}{a_B}\right) \cdot d_i, \quad (4)$$

where r denotes the distance from the core, a_B is the Bohr radius and d_i is the spherical harmonic of the corresponding d orbital. The factor χ in the exponent determines the steepness of the wave function and is determined by the Slater rules [10]. We use a value of $\chi = 2.5$ which is slightly smaller than the value determined from the Slater rules to accommodate for the partial screening of the core charges by other electrons of neighboring tip atoms.

In an isolated neutral Cu atom, the 3d shell is completely filled. In a surface atom, and in particular in the case of an exposed front atom of a tip, the tip atom is positively charged due to the Smoluchowski effect. Additionally, the 3d orbitals are not equally occupied because they are affected

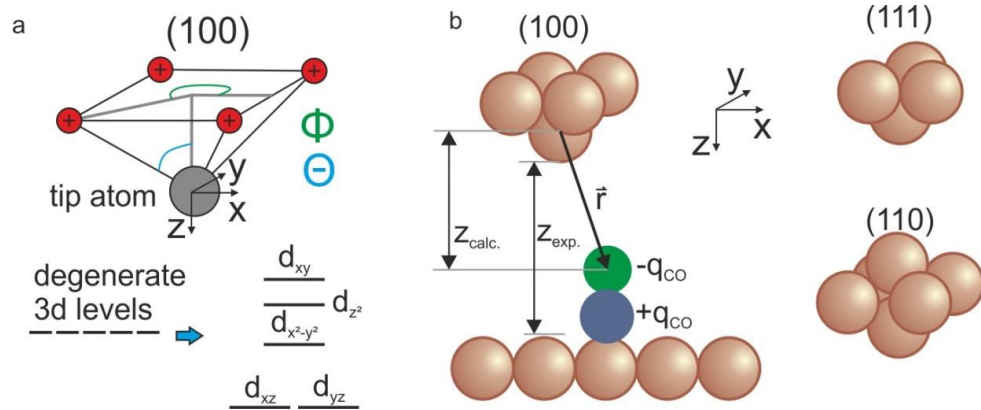


Fig. S 6 a) The crystal field of the nearest neighbors leads to a splitting of the energy levels of the 3d orbitals, as shown for the case of a Cu $\langle 110 \rangle$ tip. Angles θ and ϕ are used to calculate the overlap of each 3d orbital with the nearest neighbors. b) Tip atoms for the three tip clusters are modeled and their electrostatic interaction with the CO molecule is calculated. The origin of the coordinate system is in the center of the tip atom. The vertical height used in the calculation z_{calc} is set to the experimental value $z_{\text{exp.}}$ (see section S2).

by the partially unscreened cores of the nearest neighbors. According to crystal field theory [11] the energy levels of the 3d orbitals will split in this electric field, as illustrated in the example of a Cu<100> tip in Fig. S 6 a: An orbital which shows a large overlap with the positive charge of the nearest neighbors will be lower in energy compared to an orbital with small overlap. The relative energy splitting among the 3d orbitals is estimated with the help of the angular overlap model (AOM) [12]. In this model the overlap of an orbital with a nearest neighbor is approximated by the value of its spherical harmonic in the direction of the nearest neighbor, specified by the angles θ_i and ϕ_i (see Table 1). The overlap with the different nearest neighbors is computed by summing up their individual contributions. The number of nearest neighbors depends on the orientation of the tip cluster and is 3, 4 or 5 for the <111>, <100> or <110> directions, respectively. For example, the relative energy splitting ES for a Cu<100> tip is calculated with the following expressions:

$$\begin{aligned}
 d_{z^2} : ES_{d_{z^2}} &= 4 \frac{1}{4} (3 \cos \theta_1 - 1)^2 S_\sigma^2 \\
 d_{xz} : ES_{d_{xz}} &= 3 \sin^2(\theta_1) \cos^2(\theta_1) [\cos^2(\phi_1) + \cos^2(\phi_2) + \dots] S_\sigma^2 \\
 d_{yz} : ES_{d_{yz}} &= 3 \sin^2(\theta_1) \cos^2(\theta_1) [\sin^2(\phi_1) + \sin^2(\phi_2) + \dots] S_\sigma^2 \\
 d_{xy} : ES_{d_{xy}} &= 3 \sin^4(\theta_1) [\sin^2(\phi_1) \cos^2(\phi_1) + \sin^2(\phi_2) \cos^2(\phi_2) + \dots] S_\sigma^2 \\
 d_{xz} : ES_{d_{xz}} &= \frac{3}{4} \sin^4(\theta_1) [(1 - 2 \sin^2(\phi_1))^2 + (1 - 2 \sin^2(\phi_2))^2 + \dots] S_\sigma^2.
 \end{aligned} \tag{5}$$

The overlap factor S_σ is arbitrarily set to 1. A high ES value corresponds to a low lying energy level. We use the normalized relative energy splitting $\alpha_i = ES_i / \sum_j ES_j$ to calculate an approximation for the occupation q_{di} of the d orbitals. The d orbitals at the lowest energy level are assumed to be fully occupied with two electrons. The other orbitals are filled according to the normalized splitting energy:

$$q_{d_i} = 2e \frac{\alpha_i}{\max(\alpha_i)} . \tag{6}$$

The charge density at the tip atom is then given by the sum of probability densities of the 3d orbitals times their occupation q_{di} :

$$\rho(\vec{r}) = \sum_i q_{d_i} |\Psi_{\text{STO}}^{d_i}(\vec{r})|^2 . \tag{7}$$

The total negative charge of the tip atom is simply the sum over the occupation numbers $\sum_i q_{di}$. The total occupations of the 3d shell of the Cu tip atom are 5.33 e, 6 e and 6.65 e in the case of the

Tip orientation	θ_i	ϕ_i
100	45°	0, 90°, 180°, 270°
111	54, 73°	0, 120°, 240°
110	60°, 0°	35.26°, 144.74°, 215.26°, 324.74°

Table 1: Angles θ_i and ϕ_i in the direction of the nearest-neighbors for the three orientations of the tip cluster: The angles are used to calculate the relative shift of the energy levels and hence the occupations of the five different 3d orbitals.

Cu<100>, Cu<111> and Cu<110> tips, respectively.

Fig. S 7 shows the electron densities $\rho(x,y,z)$ for the three tip atoms. In the case of the Cu<100> tip the electron density shows a torus in the x - y plane over the whole distance regime with a lower electron density in the center. For the Cu<111> tip the electron density has the shape of a two-dimensional gaussian for large z values. Close to the center of the atom, the charge density also becomes toroidal, although its diameter is smaller compared to the Cu<100> tip. The electron density at the tip atom of the Cu<110> is not symmetric with respect to rotations around the z axis for the whole distance regime. This asymmetry is strongly enhanced for small distances. In summary, we find that the symmetry found in the COFI images is already reflected in the projections of the electron density, especially for small z values.

In the next step, we calculate the interaction of the modeled electron density with the CO molecule. We assume that the interaction can be estimated by an electrostatic potential. For this purpose, the CO molecule is modeled as a dipole with a dipole moment of $p = q_{\text{CO}} \times h = 0.1 \text{ e} \times 100 \text{ pm} = 0.48 \text{ Debye}$ (a dipole moment of $0.123 \text{ e} \times 100 \text{ pm}$ is calculated in Ref. [13] for CO/Cu) pointing away from the Cu tip (negative charge on the oxygen [13], see Fig. S 6 b). Therefore we obtain a repulsive force in regions of high electron density. Similar results are expected if the interaction was calculated by means of Pauli repulsion, as the magnitude of the repulsive force is also proportional to the electron density [14]. However, we clearly observe attractive interaction in some lateral positions and Pauli repulsion cannot fully explain the short range forces, while electrostatic interaction can.

In the electrostatic calculation the negative charge of the 3d orbitals is compensated with a positive charge in the center of the tip atom Q_{core} . By adjusting the magnitude of Q_{core} we can tune the net charge of the front atom such that realistic values (less than one electronic charge) result in spite of the partial filling of the d shells. Adjusting Q_{core} also allows to fit the force versus distance curve derived from the model potential to the experimental force curves (see Fig. 1 main text).

The model potential has the following form:

$V_{\text{tip-CO}} = V(x,y,z) - V(x,y,z+h)$ with $h = 100 \text{ pm}$ (CO modelled as a dipole with charges $\pm 0.1 \text{ e}$ spaced by a distance of 100 pm) and

$$V(x,y,z) = \frac{q_{\text{CO}}}{4\pi\epsilon_0} \left[\int_{x'=-\infty}^{\infty} dx' \int_{y'=-\infty}^{\infty} dy' \int_{z'=-\infty}^{\infty} dz' \frac{\sum_i q_{d,i} |\Psi_{\text{STO}}^{d,i}(x',y',z')|^2}{\sqrt{(x-x')^2 + (y-y')^2 + (z-z')^2}} - \frac{Q_{\text{core}}}{\sqrt{x^2 + y^2 + z^2}} \right]. \quad (8)$$

The best agreement between the model and the experimental data is obtained for core charges $Q_{\text{core}} = +5.58 \text{ e}$, $+6.52 \text{ e}$ and $+6.69 \text{ e}$ for the Cu<100>, Cu<111> and Cu<110> tips, respectively. As a result, the net charge of the tip atoms is positive for all three orientations with values of $+0.25 \text{ e}$, $+0.52 \text{ e}$ and $+0.04 \text{ e}$ for the Cu<100>, Cu<111> and Cu<110> tips, respectively.

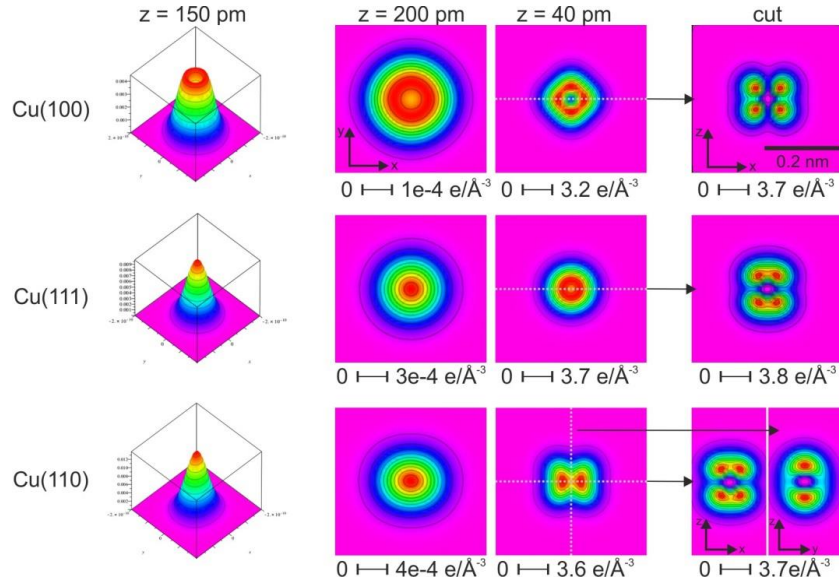


Fig. S 7 Calculated electron densities for tip atoms of Cu<100>, Cu<111> and Cu<110> tips. A 3D view and projections on the x-y and on the x-z plane (Cu<110> x-z and y-z planes) are shown. The size of the images is $400 \times 400 \text{ pm}^2$ and the center of the tip atom is in the center of the picture (with exception of the x-z/y-z image of the Cu<110> tip).

It is important to comment on the total charge of the Cu front atom here. For an isolated Cu atom, the d shell is completely filled with 10 electrons, and in our model, it is only approximately half filled. However, the total charge is still well below one elementary charge. The validity of comparing electronic states of a free atom in vacuum to an atom in bulk is of course limited – the Coulomb potential of a free atom is perfectly rotationally symmetric, while the front atom of the tip is subject to an electric field that is strongly affected by the atomic neighbors. We still trust that using free-atom states is useful and instructive, and we conjecture that the remaining d electrons might go into bulk-like states that are only weakly dependent on rotations around the z-axis of the tip.

S 6 Tip symmetries in the current image

In the CH current maps, which were acquired together with the $\langle k_{ts} \rangle$ maps, we observe a dip over the CO molecule which has approximately the shape of a cylindrical Gaussian function (Fig. S 8). However, the non-cylindrical patterns observed in the frequency shift images that mark the tip symmetries involve lateral forces, which in turn affect the shape of the current dips. The reason is that the CO molecule is bent in the force field of the tip atom, as discussed in detail in Fig. 3 and supplemental material of Ref [6]. This leads to a variation of the current minimum, as explained in Ref. [6]. We can make this variation visible by applying a Laplace filter to the current. In Fig. S 8 the result is shown for all three orientations of the Cu tip atoms. The filtered current images reveal similar features like the frequency shift maps. However, no clear difference can be observed between the Cu $\langle 100 \rangle$ and the Cu $\langle 111 \rangle$ tip. Therefore it is not possible to distinguish them by STM. Nevertheless, it is important to note that features of tip symmetry can be observed by plain STM: recording constant height images (or even topographic images) over CO molecules adsorbed on Cu (111) at distances close to the manipulation distance reveals small variations in the current- or topographic images that show up after Laplace-filtering.

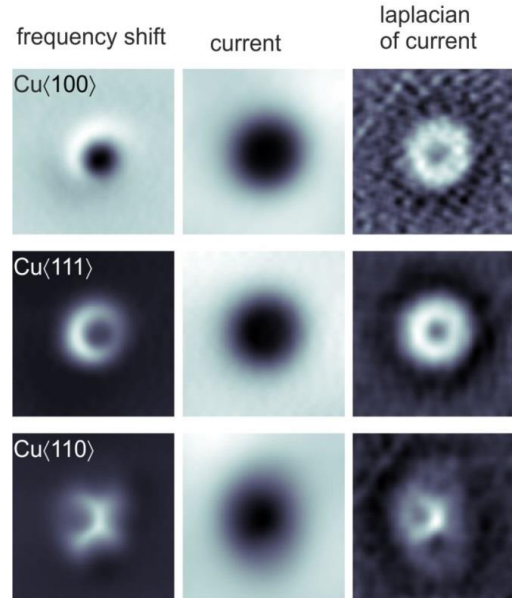


Fig. S 8: Average force gradient $\langle k_{ts} \rangle$ and current maps together with the images of the Laplace filtered current maps of the three high symmetry Cu tips.

S 7 Additional examples of COFI images of various Cu tips

Fig. S 9 shows the effect of the tilt of the tip cluster on the appearance of COFI images. Because of the random nature of tip pokes, perfect alignment in a high-symmetry direction is never achieved. However, the deviations from a perfect alignment can become small after a sufficient number of pokes (see also Fig. S 9 in Ref. [6]).

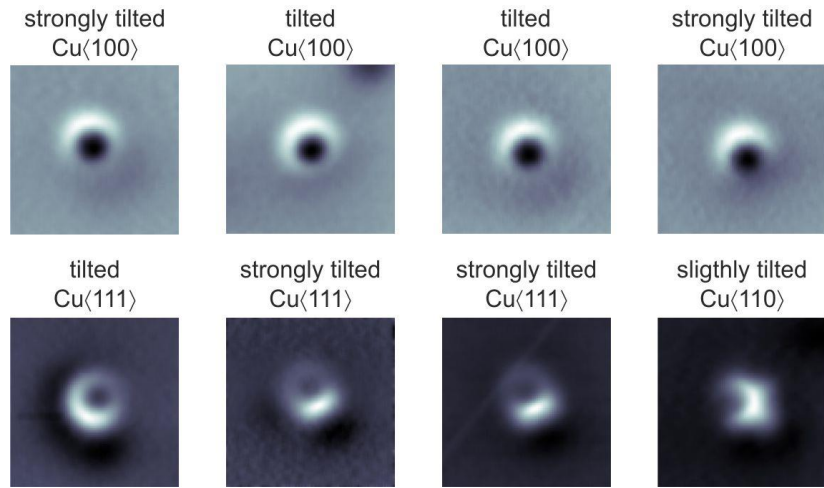


Fig. S 9 Additional examples of COFI images of various Cu tips with various tilt angles. Scan sizes are $1.5 \times 1.5 \text{ nm}^2$ for all images.

S 8 Threefold symmetries in bcc tips (Fe, W)

The highest angular momentum states of d orbitals yield a twofold symmetry with respect to rotations around the z-axis. A threefold symmetry with respect to the z axis requires f orbitals. However, it is possible to create states from d orbitals that are threefold symmetric with respect to a $\langle 111 \rangle$ axis. A linear combination of d_{xz} , d_{yz} and d_{xy} orbitals with equal weights creates a charge density proportional to $(x^2z^2 + y^2z^2 + x^2y^2)$. Such a charge density has local maxima in the $\langle 111 \rangle$ directions, i.e. along the nearest neighbor directions in bcc crystals such as W and Fe, and this charge density is threefold symmetric with respect to rotations around the $\langle 111 \rangle$ axes.

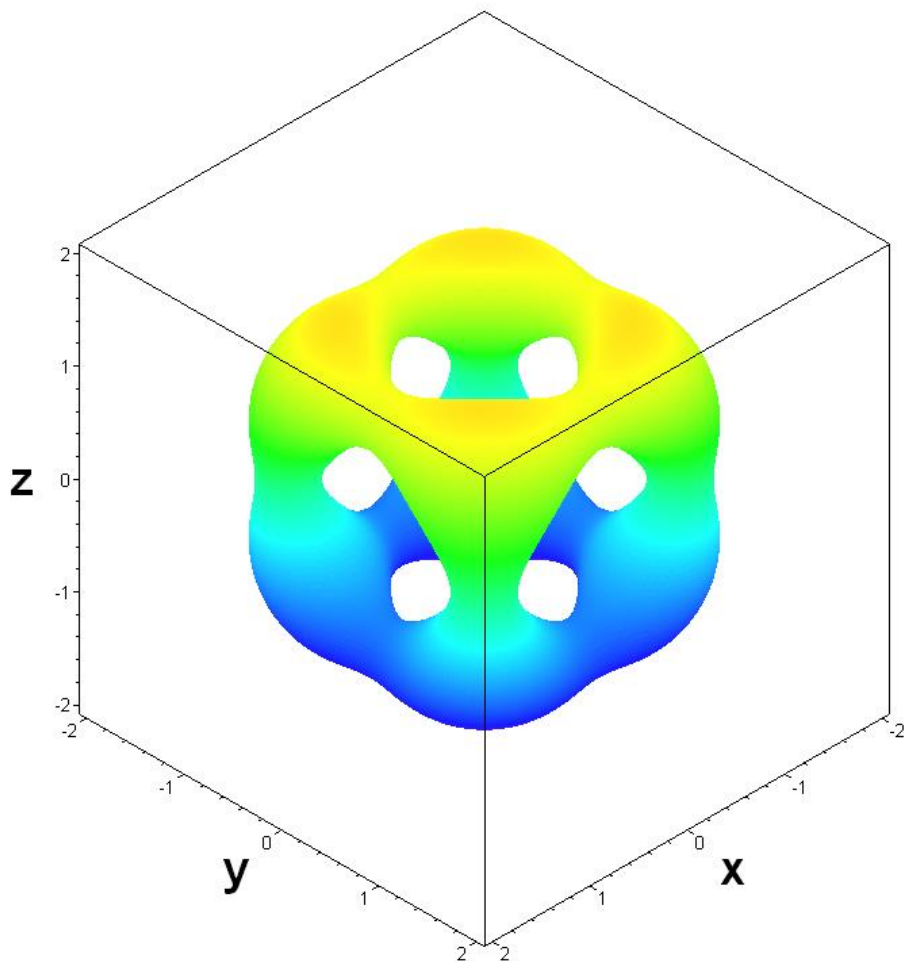


Fig. S 10 Schematic charge-density plot for a bcc tip with equally occupied d_{xz} , d_{yz} and d_{xy} states and empty $d_{x^2-y^2}$ and d_{z^2} states, yielding a charge density that is threefold symmetric with respect to rotations around a $\langle 111 \rangle$ axis.

References:

- [1] E. Müller and K. Bahadur, Phys. Rev. **102**, 624 (1956).
- [2] L. Limot, J. Kröger, R. Berndt, A. Garcia-Lekue, and W. A. Hofer, Phys. Rev. Lett. **94**, 126102 (2005).
- [3] G. Schull, T. Frederiksen, A. Arnau, D. Sánchez-Portal, and R. Berndt, Nat. Nanotechnol. **6**, 23 (2011).
- [4] F. Mohn, B. Schuler, L. Gross, and G. Meyer, Appl. Phys. Lett. **102**, 073109 (2013).
- [5] S.-W. Hla, K.-F. Braun, V. Iancu, and A. Deshpande, Nano Lett. **4**, 1997 (2004).
- [6] J. Welker and F. J. Giessibl, Science **336**, 444 (2012).
- [7] M. Ternes, C. González, C. P. Lutz, P. Hapala, F. J. Giessibl, P. Jelínek, and A. J. Heinrich, Phys. Rev. Lett. **106**, 016802 (2011).
- [8] J. E. Sader and S. P. Jarvis, Appl. Phys. Lett. **84**, 1801 (2004).
- [9] R. McWeeny, *Coulson's Valence*, 3rd Edition (Oxford University Press, Oxford, 1979).
- [10] J. Slater, Phys. Rev. **36**, 57 (1930).
- [11] J. Van Vleck, Phys. Rev. **41**, 208 (1932).
- [12] C. E. Schäffer and C. K. Jørgensen, Mol. Phys. **9**, 401 (1965).
- [13] M. Feng, P. Cabrera-Sanfelix, C. Lin, A. Arnau, D. Sánchez-Portal, J. Zhao, P. M. Echenique, and H. Petek, ACS Nano **5**, 8877 (2011).
- [14] N. Moll, L. Gross, F. Mohn, A. Curioni, and G. Meyer, New J. Phys. **14**, 083023 (2012).